Chemical Engineering Science 152 (2016) 95–108

Contents lists available at ScienceDirect

Chemical Engineering Science

journal homepage: www.elsevier.com/locate/ces

PAT-based design of agrochemical co-crystallization processes: A case-study for the selective crystallization of 1:1 and 3:2 co-crystals of p-toluenesulfonamide/triphenylphosphine oxide

K.A. Powell [a,b,*], D.M. Croker [c], C.D. Rielly [b], Z.K. Nagy [b,d]

[a] Technology Innovation Centre, University of Strathclyde, Glasgow, Lanarkshire G1 1RD, UK
[b] EPSRC Centre in Continuous Manufacturing and Crystallisation at the Department of Chemical Engineering, Loughborough University, Loughborough, Leicestershire LE11 3TU, UK
[c] Materials and Surface Science Institute and Synthesis and Solid State Pharmaceutical Centre (SSPC), University of Limerick, Ireland
[d] School of Chemical Engineering, Purdue University, West Lafayette, IN 47907, USA

HIGHLIGHTS

- Selective crystallization of p-toluenesulfonamide/triphenylphosphine oxide co-crystals.
- Application of integrated array of PAT tools to control a co-crystal formation process.
- Temperature cycling based on in situ Raman spectroscopy signal for process control.
- Use of PAT to understand solution mediated transformation events in a co-crystal system.
- Differential flow rate method demonstrated for controlling a co-crystal formation process.

GRAPHICAL ABSTRACT

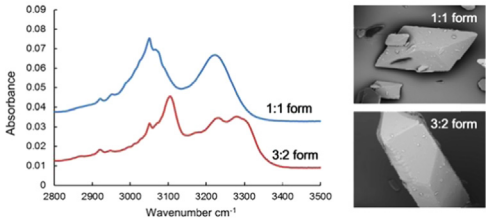

ARTICLE INFO

Article history:
Received 23 March 2016
Received in revised form
9 May 2016
Accepted 2 June 2016
Available online 3 June 2016

Keywords:
Co-crystallization
Co-crystal
Stoichiometric
Process analytical technologies

ABSTRACT

In this study, the selective crystallization and characterization of the stoichiometric forms of the p-toluenesulfonamide/triphenylphosphine oxide (p-TSA–TPPO) co-crystal system in acetonitrile (MeCN) is demonstrated using batch and semi-batch crystallizers. In the batch study, both 1:1 and 3:2 p-TSA–TPPO were successfully isolated as pure forms. However, process variability was observed in a few experimental runs. To address the batch process variability issue, a control strategy was implemented using temperature cycling, aided by in situ process analytical technologies (PAT) to convert from 3:2 to 1:1 p-TSA–TPPO. In the semi-batch co-crystallization studies, the two molecular co-formers, p-TSA and TPPO, were dissolved in MeCN and pumped separately to the crystallizer. Changing the flow rates of the respective active ingredients allowed control over the co-crystallization outcome, and presents as a promising opportunity for development of a continuous co-crystallization process.

* Corresponding author.
E-mail addresses: keddon.powell@strath.ac.uk (K.A. Powell), zknagy@purdue.edu (Z.K. Nagy).

http://dx.doi.org/10.1016/j.ces.2016.06.005
0009-2509/

1. Introduction

In the agrochemical industry there is a need for the development and application of new active ingredient design strategies to deliver solutions for the discovery of agrochemicals that are fit for purpose in the 21st century (Lamberth et al., 2013). For example, there is a need to reduce absolute usage of active agrochemical ingredients (AAIs) to minimize environmental impact. To achieve this, a structure-based design approach to AAI production is required. Structure-based design is an iterative and multi-disciplinary process that is well established in the pharmaceutical industry (Kuntz, 1992). It has played an important role in the development of several registered drugs and clinical candidates (Lamberth et al., 2013; Kuntz, 1992), for example, zanamivir (Varghese, 1999), lopinavir–ritonavir and nelfinavir (Walmsley et al., 2002). In contrast, structure-based design is a relatively new concept in the agrochemical industry, and there are currently no products on the market that are the direct result of this approach (Lamberth et al., 2013). In recent years structure-based design of multi-component molecular systems has gained popularity in the pharmaceutical sector as a viable alternative to traditional design approaches used to modify active pharmaceutical ingredients (APIs) for more effective performance. Modifications of the structure and molecular composition of an active ingredient by applying structure-based design principles can lead to significant improvements to the stability, solubility and release profile. This could lead to a reduction in use rates of AAIs, and hence a minimized environmental impact. For example, the release profile of an AAI could be controlled through the design of multi-component molecular entities such as co-crystals. Furthermore, multi-component systems offer the opportunity to delivery not just one, but two or more AAIs simultaneously, which could potentially minimize operating cost and equipment foot print through simplification of manufacturing processes.

The definition of a co-crystal has been widely debated in the scientific community (Aitipamula et al., 2012; Croker and Rasmuson, 2014), however, there is now a general consensus since the publication of FDA guidelines (FDA, 2013) that a co-crystal is a crystalline multi-component molecular entity made up of two or more components in a definite stoichiometric ratio. Co-crystallization can be an effective crystal engineering approach for modifying the crystal structure and properties of an active ingredient (Prasad and Rakesh, 2012; Sun, 2013). However, many of the current methods used to isolate co-crystal forms such as neat and liquid assisted grinding (Karki et al., 2007; Bian et al., 2013), slurry conversion (Takata et al., 2008; Croker et al., 2012), supercritical fluid enhanced atomization (Padrela et al., 2010), and evaporative co-crystallization (Croker et al., 2012; Rager and Hilfiker, 2010; Sarraguça et al., 2014) cannot be scaled to industrial production capacity. Cooling crystallization is perhaps the most viable route to scale-up, yet there are only a few studies that have explored this method to isolate co-crystals (Gagniere et al., 2009; Yu et al., 2011; Habgood et al., 2010). There are even fewer studies that are carried out using large scale laboratory crystallizers (that is, 500–1 L capacity) (Gagniere et al., 2009; Yu et al., 2011). In addition, there is limited use of process analytical technologies (PAT) to monitor, control and characterize co-crystallization processes (Sarraguça et al., 2014; Yu et al., 2011).

In this study, the co-crystallization of two model AAIs, p-toluenesulfonamide (p-TSA) and triphenylphosphine oxide (TPPO) is demonstrated as part of a proof of concept study using laboratory scale (500 mL) batch and semi-batch crystallizers. The aim of this study is to monitor, control and fully characterize the crystalline forms of the resulting multi-component AAI co-crystals using an integrated array of PAT tools, crystallization process informatics systems (CryPRINS) software, and off-line solid state characterization techniques. p-TSA and its derivatives are widely used as raw materials for the synthesis of pesticides, drugs and fluorescent colorants (Ajibola et al., 2015; Farahi et al., 2015). There are two known polymorphs of p-TSA, α form (monoclinic) differs from the β form (triclinic), which has a unusual arrangement of layers (Drebushchak et al., 2013). TPPO finds use in the production of crop protection products, anti-fungal coatings, vitamins, and APIs (Palmer et al., 2010; Richoll and Colón, 2006). There are three known polymorphic forms of TPPO (Spek, 1987; Etter and Baures, 1988), one orthorhombic and two monoclinic forms. Etter and Baures (1988) were amongst the first to isolate co-crystals of TPPO. They were able to successfully co-crystallized TPPO with 15 different molecular entities, inclusive of several derivatives of p-TSA.

There are two known stoichiometric forms of the p-TSA–TPPO co-crystal system composed of 1:1 and 3:2 mol ratios of p-TSA and TPPO respectively. There are no known polymorphic forms of these two stoichiometric co-crystal forms. Ferguson and Glidewell (1988) and Ferguson et al. (1989) isolated the 3:2 form of p-TSA–TPPO and reported on the crystal and molecular structures. The authors used a small scale reactive crystallization method whereby triphenylphosphine (TPP) was reacted with Chloramine-T(n-chloro p-toluenesulfonamide sodium salt) in ethanol; the product was then recrystallized from anhydrous benzene. Croker et al. (2012) isolated and reported the crystal structure of the 1:1 form of p-TSA–TPPO. In their work solid state grinding and small scale evaporative (10 mL) and cooling (50 mL) crystallization methods were applied. They also constructed two ternary phase diagrams at 20 °C for the two co-former molecules (p-TSA and TPPO) in acetonitrile (MeCN) and dichloromethane (CH_2Cl_2) solvents respectively. Subsequent studies examined the nucleation behavior (Croker et al., 2013a), isothermal suspension conversion (Croker and Rasmuson, 2014) and solution-mediated phase transformation (Croker et al., 2013b) of the two co-crystal forms.

In this study, a control strategy employing a temperature cycling approach was implemented in the batch cooling co-crystallization process where variability was detected. This was aided by an integrated array of PAT tools consisting of Raman, attenuated total reflectance ultra-violet/visible (ATR-UV/vis) and Fourier transform infrared (ATR-FTIR) spectroscopy, focused beam reflectance measurement (FBRM) and particle vision microscopy (PVM) with complementary solid state characterization techniques were used for intelligent decision support (IDS) and control of the co-crystallization processes using the crystallization process informatics system (CryPRINS). Complementary off-line solid state characterization techniques, comprising powder X-ray diffraction (PXRD), differential scanning calorimetry (DSC), hot stage microscopy (HSM), scanning electron microscopy/energy dispersive spectroscopy (SEM), Raman microscopy and FTIR spectroscopy were used for phase identification. In the semi-batch operation, a flow rate control strategy also aided by PAT and off-line analysis, whereby the two co-formers are dissolved and pumped separately to a crystallizer unit was demonstrated as a viable option for controlling the co-crystallization outcome. This approach shows promise for further development into a continuous co-crystallization process. The batch and semi-batch co-crystallization studies at a larger scale (500 mL) compared to previous works to examine the scalability of the p-TSA–TPPO system. A further aim of the study is to monitor and control the selective co-crystallization of the 1:1 and 3:2 co-crystal forms of the p-TSA–TPPO system, applying the array of PAT tools to gain better process understanding.

2. Materials and methods

2.1. Chemicals

Crystallizations were carried out using MeCN as solvent and the resulting co-crystal complexes, 1:1 p-TSA–TPPO and 3:2 p-TSA–TPPO

characterized using different solid-state techniques. Fig. 1 shows the chemical structures of the starting materials (top) and crystal structures of the co-crystals (bottom). Acetonitrile (MeCN, Analytical Reagent Grade, 99.9%) was obtained from Fisher Scientific, UK. p-Toluenesulfonamide (p-TSA, 99%) and triphenylphosphine oxide (TPPO, 99%) were obtained from Sigma-Aldrich, UK and used as received. The structure of 1:1 p-TSA–TPPO consists of cyclic centrosymmetric aggregates in which two molecules of p-TSA are linked to two molecules of TPPO via two point hydrogen bonds of the type:O——H–N(SO_2Ph)–H——O: as shown in Fig. 1, with a lone pair of electrons on the oxygen of TPPO. The 3:2 p-TSA–TPPO co-crystal is also made up of cyclic centrosymmetric aggregates, but with three molecules of p-TSA linked to two molecules of TPPO via a network of six linear hydrogen bonds of the type O——H–N(SO_2Ph)–H——O, with no lone pair electrons on the oxygen of TPPO.

In this study, the ternary phase diagram of p-TSA/TPPO/MeCN at 20 °C, Fig. 2, developed by Croker et al. (2012) was used as a guide for producing pure 1:1 and 3:2 p-TSA–TPPO co-crystal forms (Regions 1 and 2), and mixtures (Region 3), albeit at different operating temperatures. The study aims to demonstrate that control over the co-crystallization process in batch and semi-batch crystallizer platforms is possible even under different operating conditions.

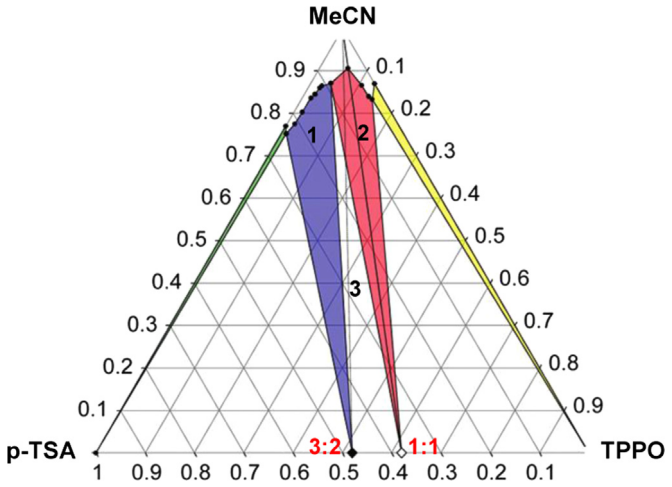

Fig. 2. Ternary phase diagram (axes in mass fraction) for the p-TSA/TPPO/MeCN at 20 °C. (1) 3:2 co-crystal form stable; (2) 1:1 co-crystal form stable; (3) mixtures of 1:1 and 3:2 forms stable. Adopted from Croker et al. (2012).

2.2. Solid state characterization

Powder X-ray diffraction (PXRD) studies were carried out using a Bruker D2 Phaser bench-top X-ray diffractometer with Cu K_α radiation source. A 3 mm anti-scatter slit was used with a programmable divergent slit of 1 mm. A 1.5° Soller slit was employed and diffractograms were collected between 5° and 90° 2θ with a step size of 0.02°. In preparation for PXRD analysis, samples were mounted and spread evenly onto 12 mm disks.

A Thermo Scientific DXR™ Raman Microscope equipped with 780 nm laser, Olympus TH4 200 optical component, and Linkam THMS600 heating/freezing stage was used for phase identification, polymorph characterization and image analysis. The full spectral range of the instrument (50–3500 cm^{-1}) was captured with a single exposure of the charged-coupled-device (CCD). Samples for polymorph screening and imaging were mounted on glass slides and analyzed using either, 4 ×, 10 × or 50 × objective, resulting in spot sizes of 7.9, 3.8 and 1.3 μm respectively. Raman spectra were collected using the 50 μm slit and a laser setting of 15 mW. The number of scans and exposure time for each sample was 10 × 10 s. The instrument settings led to estimated resolution of 4.7–8.7 cm^{-1}. Data processing and analysis was carried out using Thermo Scientific OMNIC™ Series Raman software and TQAnalyst™ version 8.0 software.

Hot stage microscopy (HSM) studies were carried out using the Linkam THMS600 unit. The stage body fitted quick-to-fit gas port was connected to a LNP95 cooling pump to control the sample atmosphere using a dry nitrogen flow. Samples were loaded onto a 0.17 mm thick cover slip and placed on a highly polished pure silver heating element to ensure good heat transfer and sensitive temperature measurements. Samples were equilibrated at 100 °C, followed by controlled heating at a rate of 1 °C/min to 180 °C. Images were captured whenever phase changes were detected.

A Thermo Scientific Nicolet™ iS™50 FT-IR benchtop spectrometer with a KBr beam splitter and DTGS ATR detector was used as a complementary tool to Raman spectroscopy for phase identification and polymorph characterization. The spectral range of the instrument was 400–4000 cm^{-1}. Prior to analysis a background

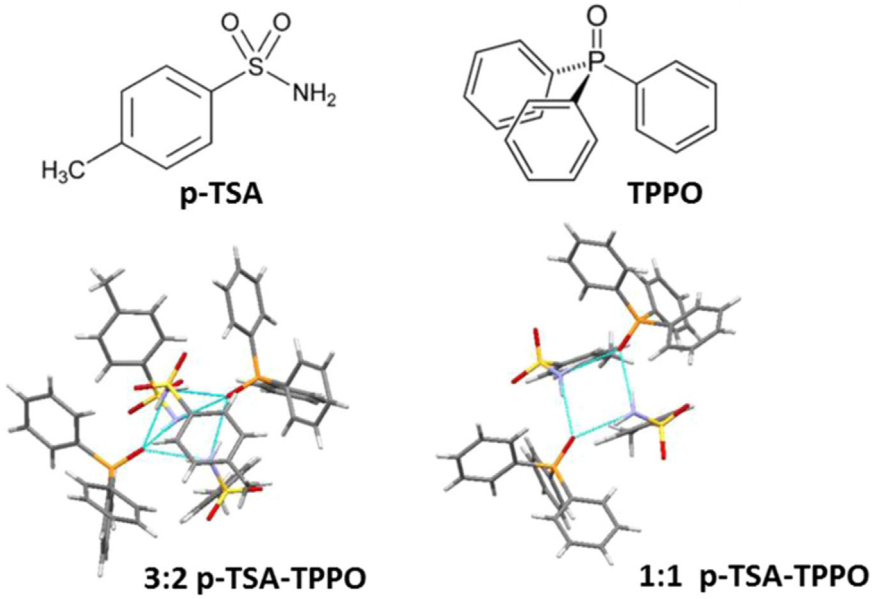

Fig. 1. Chemical structures of p-TSA and TPPO (top) and crystal structures of 1:1 and 3:2 p-TSA–TPPO co-crystals (bottom). Adopted from Croker and Rasmuson (2014).

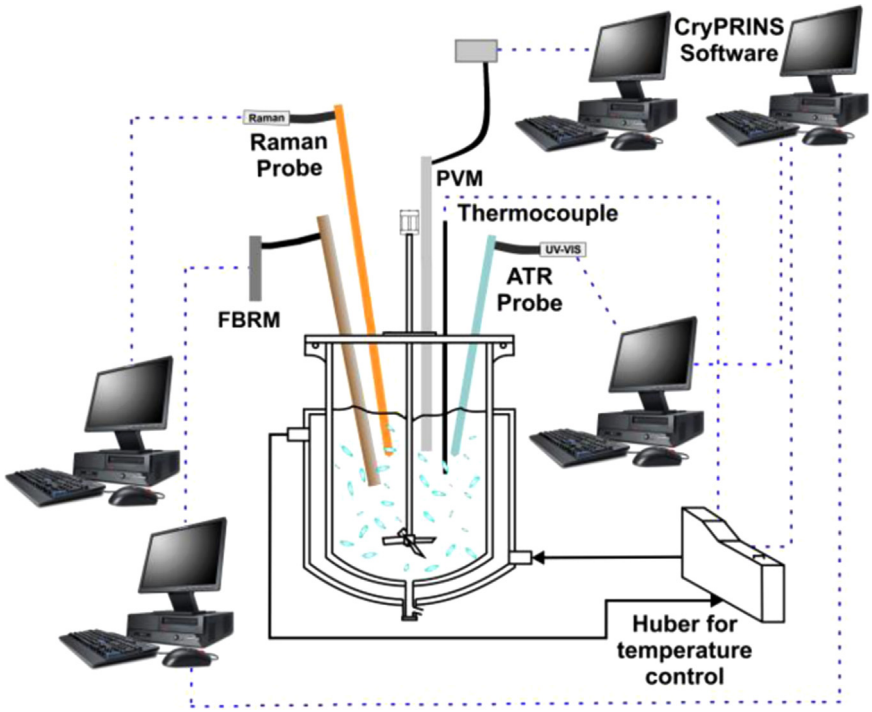

Fig. 3. Schematic of batch crystallizer used for the cooling co-crystallization experiments.

reading (5 scans averaged) was taken in air to eliminate interferences from CO_2, H_2O and other atmospheric gases. Samples were then mounted on the ATR iS50 window and fixed in place using a sample holder supplied with the instrument. The instrument was set to absorbance mode and 10 scans were recorded and averaged over 10 seconds for each sample, leading to a spectral resolution of 4 cm^{-1}. Data processing and analysis was carried out using Thermo Scientific OMNIC™ Series FT-IR software and TQAnalyst™ version 8.0 software.

DSC analyses were carried out using a Thermal Advantage DSC Q20 fitted with a Thermal Advantage 90 cooling system, using nitrogen gas at a flow rate of 18 cm^3/min. Each sample was equilibrated at 40 °C for 2 min followed by heating at a rate of 5 °C/min to 250 °C. Data were collected and processed using the Instruments-Waters LLC Advantage Qseries version 5.4.0 software package supplied with the instrument.

Scanning Electron Microscopy (SEM) studies were carried out using a Carl Zeiss 1530 VP high resolution field emission gun scanning electron microscope (FEGSEM). Samples were prepared for SEM analysis using a bench-top Quorum Q150T ES gold sputter coater/carbon evaporator coating system with turbo-molecular pump. The system was used to coat each sample with a thin film of gold-palladium prior to analysis.

HPLC analyses were performed using a Hewlett Packard HP1100 Series chromatograph with a DAD.G1315A diode array detector using a Waters Spherisorb C8 Column (80 Å, 5 μm, 4.6 mm × 250 mm) eluting with MeCN:H_2O (80:20) at 1 mL/min and UV detection at 254 nm.

2.3. Batch co-crystallization study

Small scale batch co-crystallization studies (1–50 mL) on the p-TSA–TPPO system have previous been reported (Croker and Rasmuson, 2014; Croker et al., 2012, 2013a). The co-crystallization experiments were carried out in a 500 mL jacketed glass vessel fitted with an overhead PTFE pitch blade stirrer. The jacket was connected to a Thermofluid bath (Huber ministat 230) for temperature control. Temperature profiles were implemented and data recorded using CryPRINS software (version 2.0). A RXN1 Raman spectrometer from Kaiser Optical Inc. with 785 nm laser source and immersion probe was used for in situ real-time monitoring of the co-crystal forms of p-TSA–TPPO. FBRM® D600 and PVM® instruments from Mettler Toledo were used for nucleation and dissolution detection, and to tracking the evolution of crystal properties (size shape and distribution). An ATR-UV/vis spectrometer fitted with Helma 661.820-UV immersion probe or Thermofisher FTIR spectrometer fitted with artphotonics ATR Silicium SN 210 immersion probe was used to monitor changes in the solution phase. A schematic representation of the experimental set-up used is shown in Fig. 3.

For each experimental run, the required amount of p-TSA, TPPO and MeCN were added to the reactor and heated to 30, 60 or 70 °C to dissolve the solids (depending on the initial loading of starting materials) at a rate of 1 °C/min. The vessel was held for 15 min to allow complete dissolution of the materials, followed by cooling at a rate of −1.0 °C/min to a final temperature of either 20 or 5 °C, and holding for 1 h (experiments 1–4). For experiments 5–9 ramped temperature profiles were implemented, the heating/cooling rate regime was 0.2/−0.2 °C/min. The impeller speed for all experiments was set to 400 rpm, which corresponds to an approximate power per unit volume of 0.075 kW/m^3. Table 1 gives a summary of the experimental conditions for each run. The material from each experimental run was isolated at the end of the batch time by vacuum filtration. The wet solid collected was then dried overnight at 40 °C.

2.4. Semi-batch co-crystallization study

A series of semi-batch development experiments were performed to determine the most suitable conditions for the selective crystallization of the 1:1 and 3:2 stoichiometric co-crystal forms of the p-TSA–TPPO co-crystals system. The combination of p-TSA/TPPO/MeCN was varied on a mass fraction basis by changing the flow rate of each co-former. All experiments were carried out using the experimental set-up described in Section 2.1 (Fig. 3). The required amount of p-TSA and TPPO were dissolved in separate

Table 1
Summary of experimental conditions employed during the batch crystallization of p-TSA–TPPO co-crystals.

Exp no.	p-TSA (g/g MeCN)	TPPO (g/g MeCN)	Temperature (°C)		Heating/Cooling rates (°C/min)	Component mass fractions (M)			Region of phase diagram at 20 °C
			Initial	Final		p-TSA	TPPO	MeCN	
1	0.1147	0.1532	60	20/5[a]	1.0/−1.0	0.09	0.12	0.79	2 (1:1 form)
2	0.2634	0.1247	60	20/5[a]	1.0/−1.0	0.19	0.09	0.72	1 (3:2 form)
3	0.5776	0.4202	70	5	1.0/−1.0	0.29	0.21	0.50	1 (3:2 form)
4	0.3793	0.6193	70	5	1.0/−1.0	0.19	0.31	0.50	2 (1:1 form)
5	0.0706	0.1059	30	5	0.2/−0.2	0.06	0.09	0.85	2 (1:1 form)
(6)	0.1728	0.0617	30	5	0.2/−0.2	0.14	0.05	0.81	1 (3:2 form)
(7)	0.1049	0.0968	30	20	0.2/−0.2	0.09	0.08	0.83	3 (mixture)
8	0.1084	0.0964	30	20	0.2/−0.2	0.09	0.08	0.83	3 (mixture)
9	0.0833	0.1071	30	5	0.2/−0.2	0.07	0.09	0.84	2 (1:1 form)

[a] Cooled to 20 °C and held for 60 min, followed by cooling to 5 °C and holding for 60 min; ( ) temperature cycles implemented.

vessels to generate undersaturated solutions according to Table 2. Solutions were prepared by heating suspensions of p-TSA and TPPO in MeCN to 30 °C and then holding for 15 min to allow complete dissolution of the materials. The resulting solutions were then cooled to 25 °C and pumped separately to the 500 mL crystallizer vessel kept at 20 °C. Fig. 4 shows a flow diagram of the experimental set-up used.

Calibrated and pre-programmed Masteflex® pumps fitted with 3.1 mm ID platinum cured tubing were used to pump p-TSA–MeCN and TPPO–MeCN solutions to the batch crystallizer. The flow rates of p-TSA and TPPO solutions were varied from 15 to 32.7 g/min and 20 to 37.7 g/min respectively. The targeted combined flow rate of the two streams was 52.7 g/min for each experimental run. Pumps were programmed to operate for 6.71 min, leading to the delivery of approximately 493 mL of combined p-TSA–TPPO–MeCN solution to the crystallizer, which was initially empty. A holding period of approximately 60 min was implemented after the crystallizer was filled. For all experiments, the impeller speed of the crystallizer was set to 400 rpm. Table 2 provides a summary of the conditions employed during each experimental run.

3. Results and discussion

The ternary phase diagram for p-TSA/TPPO/MeCN was constructed and fully explored by Croker et al. (2012) using small scale experiments. In the current work, the mass fractions of p-TSA/TPPO/MeCN were varied according to the ternary phase diagram shown in Fig. 2. The phase diagram was used as a guide to selecting conditions that favor the formation of either the 3:2 or 1:1 co-crystal forms, as well as conditions that favor the formation of mixtures of the two forms.

3.1. Solid state and solution phase characterization

The raw materials p-TSA, TPPO and MeCN were characterized both in the solid phase (using PXRD, off-line Raman and ATR-FTIR spectroscopy, HPLC, DSC and SEM) and solution phase (using in situ Raman spectroscopy). The solid and liquid phase characterizations were later compared to samples acquired from each of the batch experimental runs. In house reference samples for the 1:1 and 3:2 p-TSA–TPPO co-crystal forms were prepared according to the procedures of Croker et al. (2012, 2013a), solid state characterizations were carried out using the techniques described earlier.

3.1.1. PXRD, Raman microscopy, ATR-FTIR and DSC analyses

Fig. 5(a)–(d) shows the patterns obtained from PXRD (a), Raman (b), ATR-FTIR (c), and DSC (d) solid state characterizations of the starting materials and co-crystal reference material, respectively. For each material analyzed, the patterns show distinctive features that were exploited to identify subsequent samples collected from different experimental runs during the study.

Clear differences are observed between the co-crystal forms and their respective starting materials and physical mixture. For example, The PXRD patterns show distinctive broad (1:1 p-TSA–TPPO) and sharp (3:2 p-TSA–TPPO) peaks in the 2-Theta (°) positions 7–10 and 17–22. The Raman spectra show differences in peak width and position in the regions 3180–2855, 1150–890, and 780–480 cm^{-1}. In terms of the ATR-FTIR signal, 1:1 and 3:2 p-TSA–TPPO both show distinctive broad peaks in the region 3400–3100 cm^{-1}. Distinctive differences between the two forms are also observed in the fingerprint region from 1500 to 400 cm^{-1}. The DSC patterns also show the clear difference between the melt of the two co-crystals, their parent compounds and physical mixture. The melts for the different crystalline phases are observed at approximately 140 °C (1:1 p-TSA–TPPO), 144 °C (3:2 p-TSA–TPPO), 139 °C (p-TSA) and 159 °C (TPPO). Interestingly, the physical mixture of p-TSA and TPPO shows a very broad endotherm from approximately 121–140 °C. It is unclear why there is such a significant shift in the endotherm for the physical mixture of the two compounds. DSC scans from replicate runs showed a similar profile, which suggests that heating the two

Table 2
Summary of experimental conditions employed during the semi-batch crystallization of p-TSA–TPPO co-crystals.

Exp no.	p-TSA (g/g MeCN)	TPPO (g/g MeCN)	Solution flow rates (g/min)		Mass fractions (M) in crystallizer			Region of phase diagram at 20 °C
			p-TSA soln.	TPPO soln.	p-TSA	TPPO	MeCN	
10	0.2987	0.1482	28	24.7	0.12	0.09	0.79	1 (3:2 form)
11	0.2987	0.1482	32.7	20.0	0.14	0.05	0.81	1 (3:2 form)
12	0.2987	0.1482	20.0	32.7	0.09	0.08	0.83	3 (mixture)
13	0.2987	0.1482	15.0	37.7	0.06	0.09	0.85	2 (1:1 form)
14	0.4625	0.2016	20.0	32.7	0.12	0.12	0.76	2 (1:1 form)
15	0.2987	0.1482	23.4	29.3	0.10	0.08	0.83	3 (mixture)
16	0.2987	0.1482	17.7	35	0.08	0.08	0.84	3 (mixture)
17	0.2987	0.1482	27.5	25.2	0.11	0.07	0.82	1 (3:2 form)

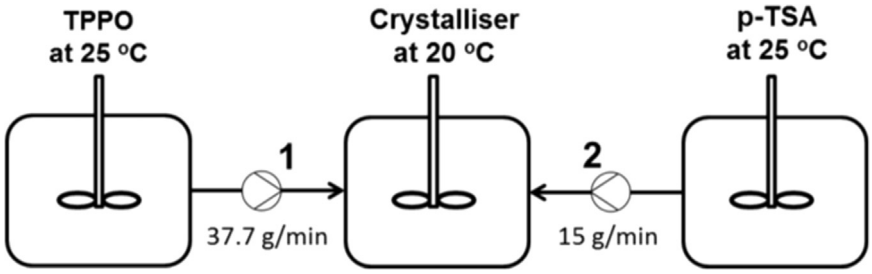

Fig. 4. Flow diagram showing the configuration of the semi-batch experimental set-up used during the co-crystallization studies.

substances together leads either to the lowering of both of their melting points or the formation of different crystalline phase, which has a lower melting point. However, these hypotheses require further investigations, which are beyond the scope of the current study.

3.1.2. HPLC analyses

Samples from each of the experimental runs performed during this study were characterized using the solid state techniques described above, and the resulting patterns compared to the raw material and reference patterns, as shown in Fig. 5. The purity and stoichiometric composition of the 1:1 and 3:2 p-TSA–TPPO co-crystal forms was confirmed by HPLC, applying a univariate calibration model developed by preparing different mass fractions of the starting materials (p-TSA and TPPO) in MeCN and finding the ratio between the areas of the resolved peaks of both components. Fig. 6 shows the calibration curve used to determine the relative amount of p TSA and TPPO in samples obtained from each experimental run. The regions corresponding to 1:1 and 3:2 p-TSA–TPPO (i.e. based on % Mass TPPO) are indicated by dashed lines.

3.1.3. HSM analyses

Hot stage microscopy studies we carried out on co-crystal samples obtained from selected experimental runs. Fig. 7(a) and (b) shows the images captured from 100 °C until 148 °C (left) and DSC scans (right) for the melting of 3:2 and 1:1 p-TSA–TPPO. For the hot stage microscopy study, melting was observed in the temperature ranges 141–148 °C, and 139–143 °C for 3:2 p-TSA–TPPO, and 1:1 p-TSA–TPPO, respectively, showing good agreement with DSC which gave melting points of 143.7 °C and 139.9 °C for the respective co-crystal forms. The additional endothermic event at 128.2 °C observed in the 3:2 co-crystal profile is most likely residual starting material since this peak seems to correspond to the melt of physical mixture of p-TSA and TPPO as shown in Fig. 5 (d). All analytical tools (off-line and on-line) used in the study indicated pure 3:2 p-TSA–TPPO including HPLC.

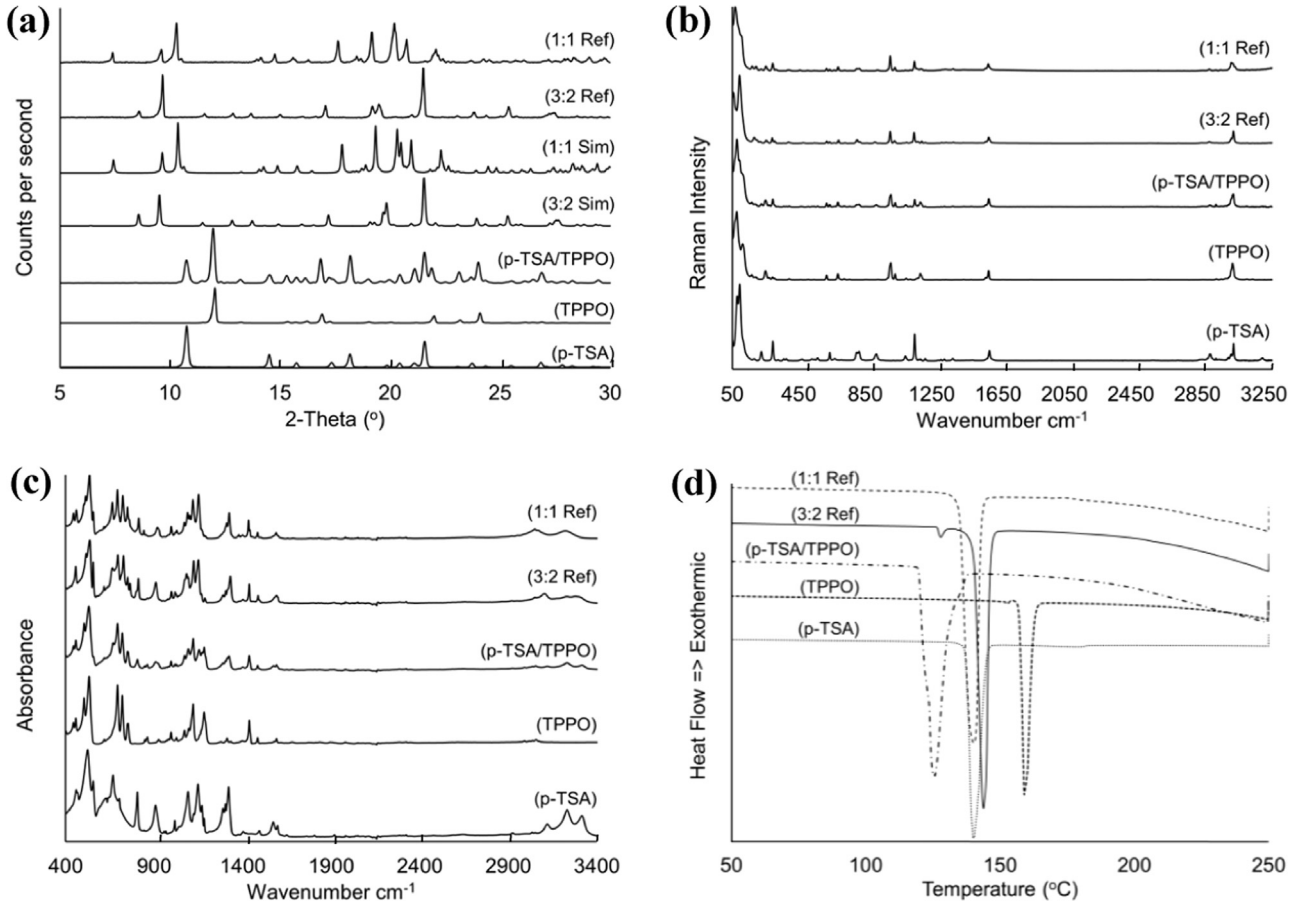

Fig. 5. Solid state characterization results for p-TSA, TPPO and 1:1 co-crystal reference, 3:2 reference, 1:1 co-crystal simulated and 3:2 co-crystal simulated, showing: (a) PXRD patterns; (b) Raman spectra; (c) ATR-FTIR spectra; and (d) DSC patterns.

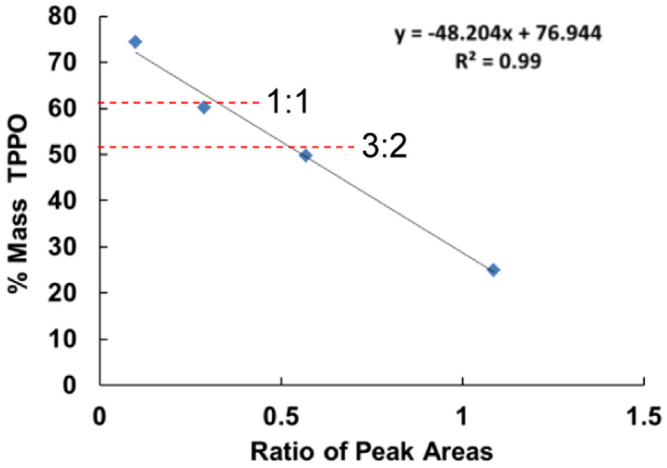

Fig. 6. Univariate HPLC calibration model used to determining the purity and stoichiometry of 1:1 and 3:2 p-TSA–TPPO co-crystal forms.

3.1.4. SEM analyses

Fig. 8(a)–(d) shows SEM micrographs (60 × magnification) of samples with different co-crystal compositions. The distinct morphology of the 1:1 and 3:2 p-TSA–TPPO is evident from the SEM micrographs. In particular, Fig. 8, images (e) (300 ×) and (f) (400 ×) show clearly the rhombic and rod shapes of the 1:1 (e) and 3:2 (f) crystalline forms of p-TSA–TPPO, respectively. Fig. 8 (c) and (d) obtained from two different experimental runs show a clear distinction in crystal size, which is attributed to a difference in the mass fraction composition of materials in the batch crystallizer (which is related to the supersaturation). This leads to different crystal sizes, which suggests that the mass fraction composition of materials in the crystalliser can be adjusted to control the mean size and CSD of the final product.

Using the equilibrium solubility (Croker et al., 2012) at the crystalliser operating temperature (20 °C), the supersaturation with respect to 1:1 p-TSA–TPPO for these two experiments works out to 2.94 (c) and 1.77 (d), respectively. It appears that the growth of the crystals is extremely fast and is favored at low

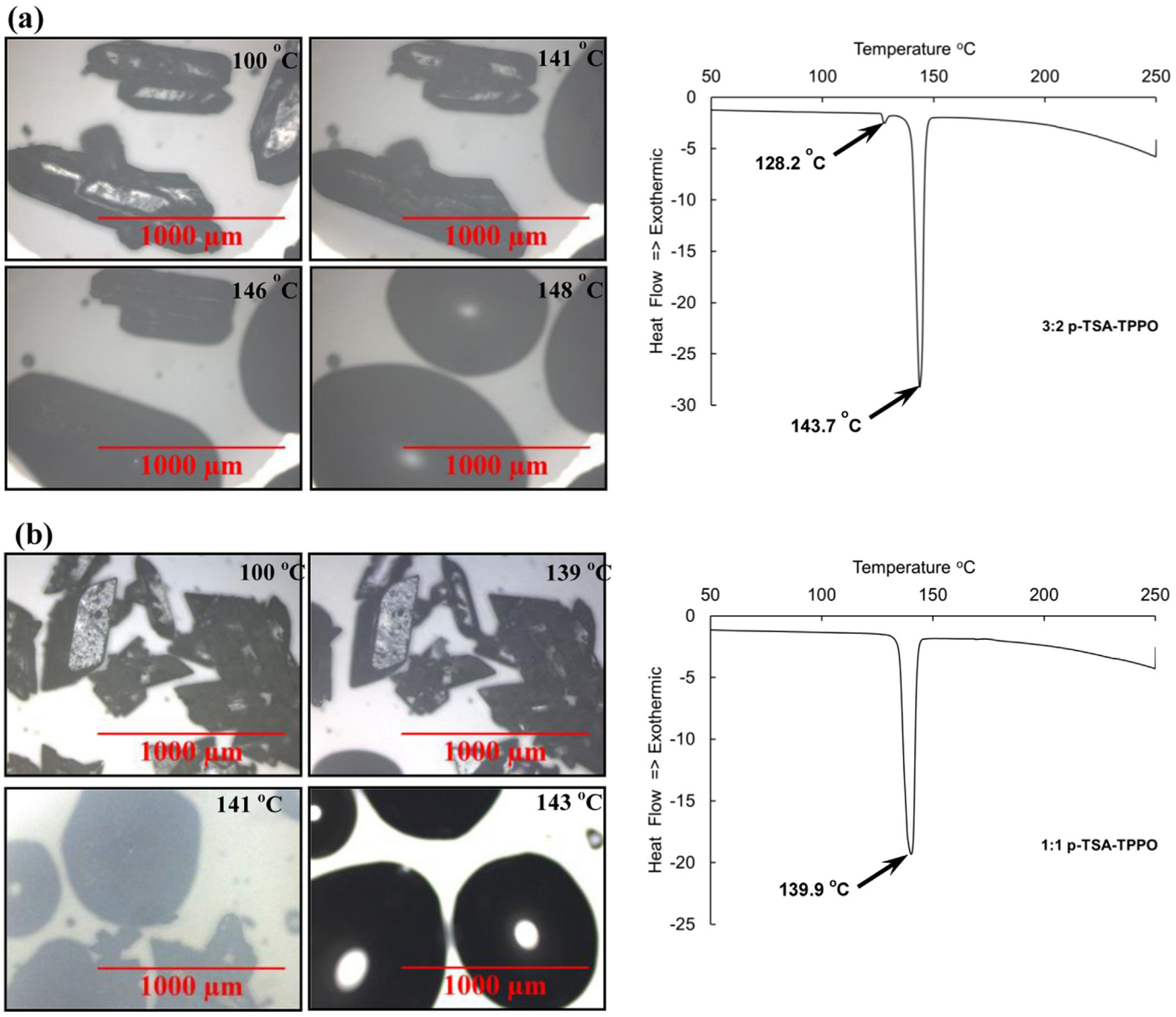

Fig. 7. Hot stage microscopy images (left), (a) 1:1 p-TSA–TPPO and (b) 3:2 p TSA–TPPO; and respective DSC scans (right) for each sample.

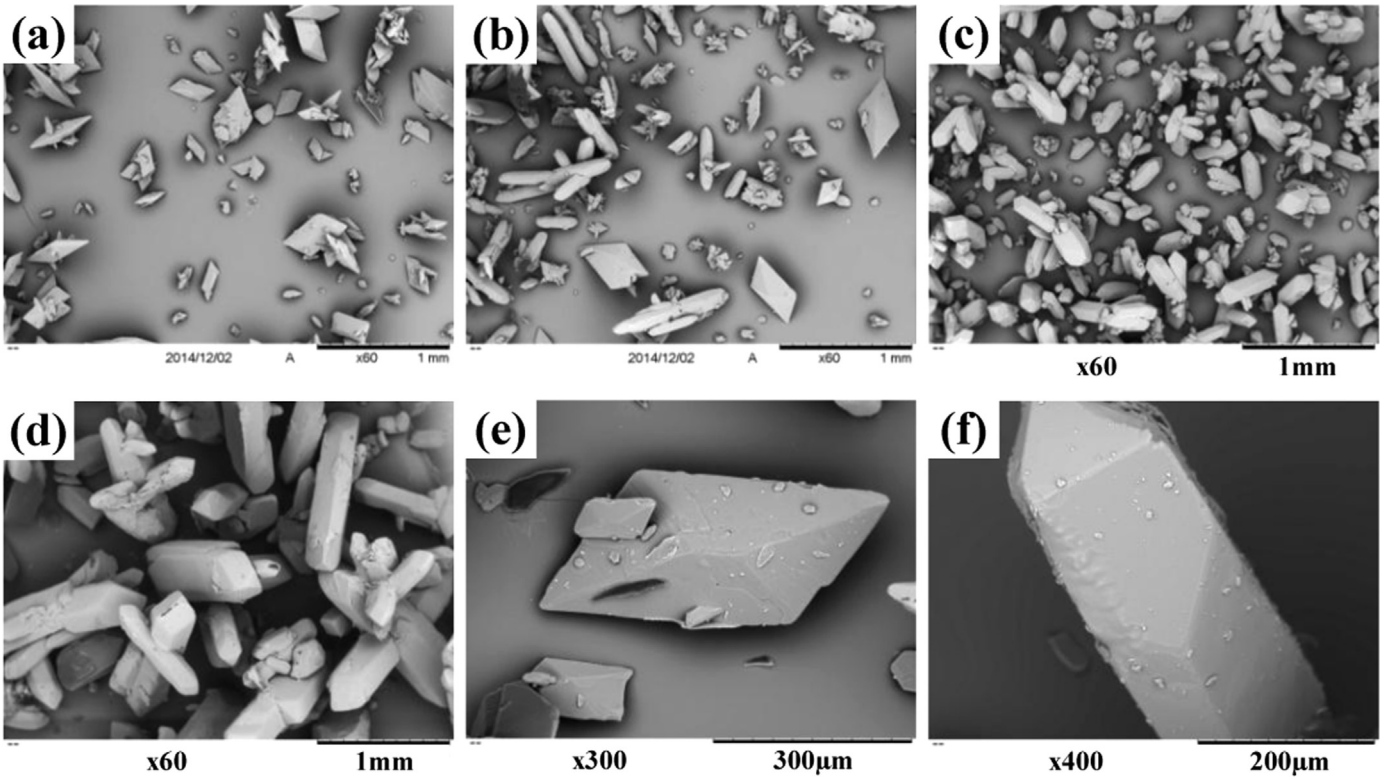

Fig. 8. SEM micrographs of (a) 1:1 p-TSA–TPPO (60 ×); (b) mixture of 1:1 and 3:2 p-TSA–TPPO (60 ×); (c) and (d) 3:2 p-TSA–TPPO (60 ×); and (e) 1:1 p-TSA–TPPO (300 ×) and (f) 3:2 p TSA TPPO (400 ×) crystals.

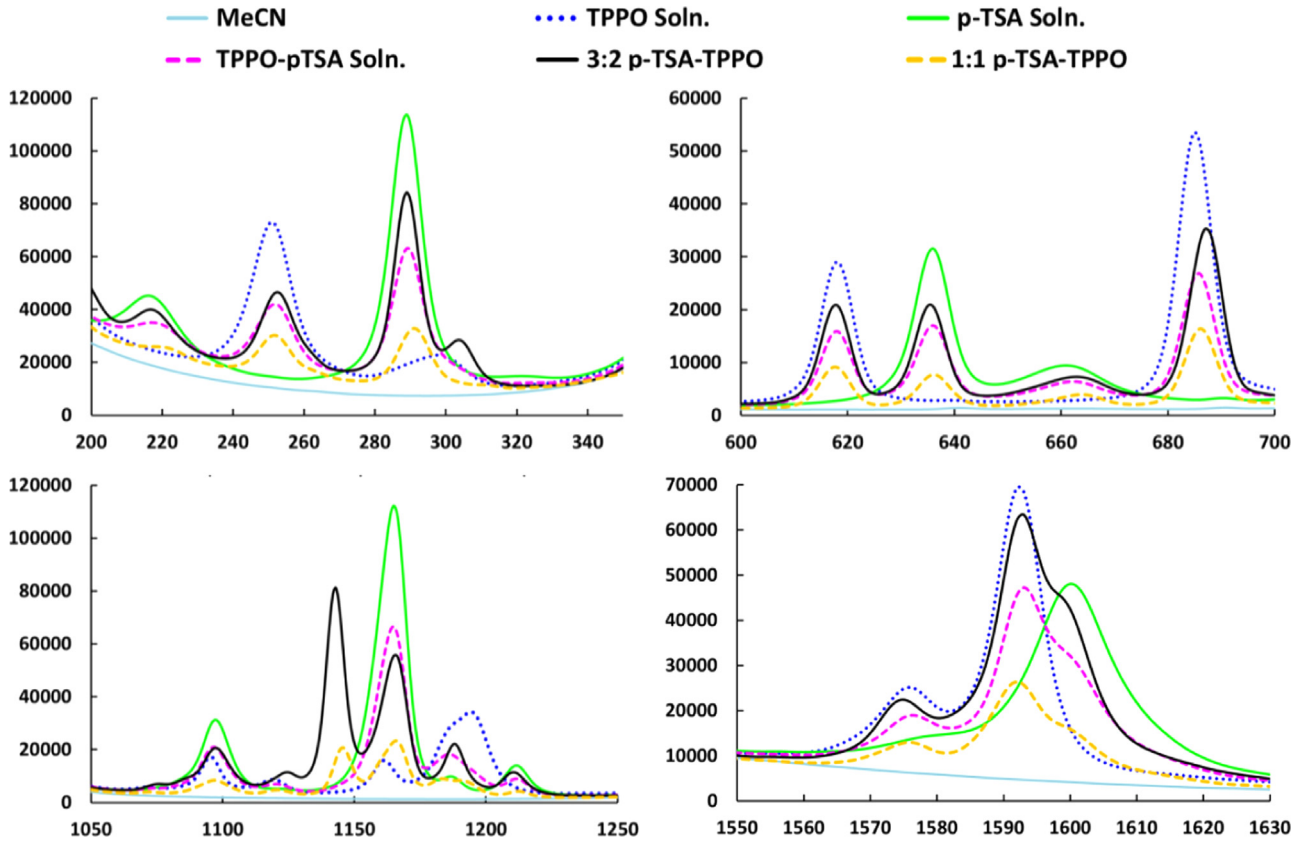

Fig. 9. Regions of in situ Raman spectra used to differentiate between solution and solid phases of the p-TSA/TPPO/MeCN system.

supersaturation (d) compared to higher supersaturation (c), which is expected. However, the supersaturation of the former is still quite high, which suggest that the 3:2 co-crystal phase is extremely fast growing as crystals greater than 1 mm size were observed.

3.2. In situ process monitoring and characterization

Real-time in process characterizations were carried out applying in situ Raman and ATR-FTIR spectroscopy to clear solutions and suspensions of 1:1 and 3:2 p-TSA–TPPO, respectively. Fig. 9 shows the regions selected from Raman spectroscopy for identification of the different phases. Results from each of the co crystallization runs were routinely correlated with HPLC measurements on samples taken at different intervals in order to confirm the identity of the solid forms present. Where necessary, other off-line measurement techniques as described earlier in Sections 2.2 and 3.1 were also employed to validate the results from the in situ process measurements and HPLC, for example, in cases where a mixture of different crystalline forms were suspected. This study highlights the complementarity of off-line and in situ process measurements. Furthermore the application of both methods provides a robust analysis of the co-crystallization process as well as valuable information for process scale-up.

In Fig. 9 the Raman spectral bands in the regions 200–350, 600–700, 1050–1250 and 1550–1610 cm^{-1} correspond, respectively, to modes of aromatic ring wagging (233–262 cm^{-1}), C–N bending (289–304 cm^{-1}), ring C–H and ring out-of-plane bending (710–770 cm^{-1}), N–H bending and ring C–H bending (784–825 cm^{-1}), C–C ring stretching and C–S stretching (1083–1110 cm^{-1}), P=O symmetric and asymmetric stretching (1130–1200 cm^{-1}) and aromatic ring vibrations (1560–1620 cm^{-1}) (Socrates, 2001).

It has been shown so far that off-line solid-state and in situ characterization techniques can be applied effectively to distinguish between the different crystalline forms of p-TSA and TPPO, including their stoichiometric co-crystal forms. This information can be applied not only to distinguish between crystalline forms, but also to inform the development of effective crystallization control strategies in batch, semi-match and periodic flow crystallizers.

3.3. Batch co-crystallization monitoring and control

The batch cooling co-crystallization of p-TSA and TPPO to give stoichiometric 1:1 and 3:2 p-TSA–TPPO co-crystal forms was monitored by applying an integrated PAT array (Fig. 3) to extract information pertaining to the stability of each co-crystal form under different operating conditions. A further aim was to optimize the batch process for the selective crystallization of each co-crystal form, achieved by tuning either the starting composition of p-TSA/TPPO/MeCN or the crystallization temperature profile. Fig. 10 (a) and (b) shows the process time diagrams obtained from monitoring the crystallization of 1:1 and 3:2 p-TSA–TPPO during experiments 1 and 2 (Table 1) respectively using FBRM, ATR-UV/vis and ATR-FTIR spectroscopy. Also shown are the microscope images of the crystalline products. The 1:1 form of p-TSA–TPPO show a

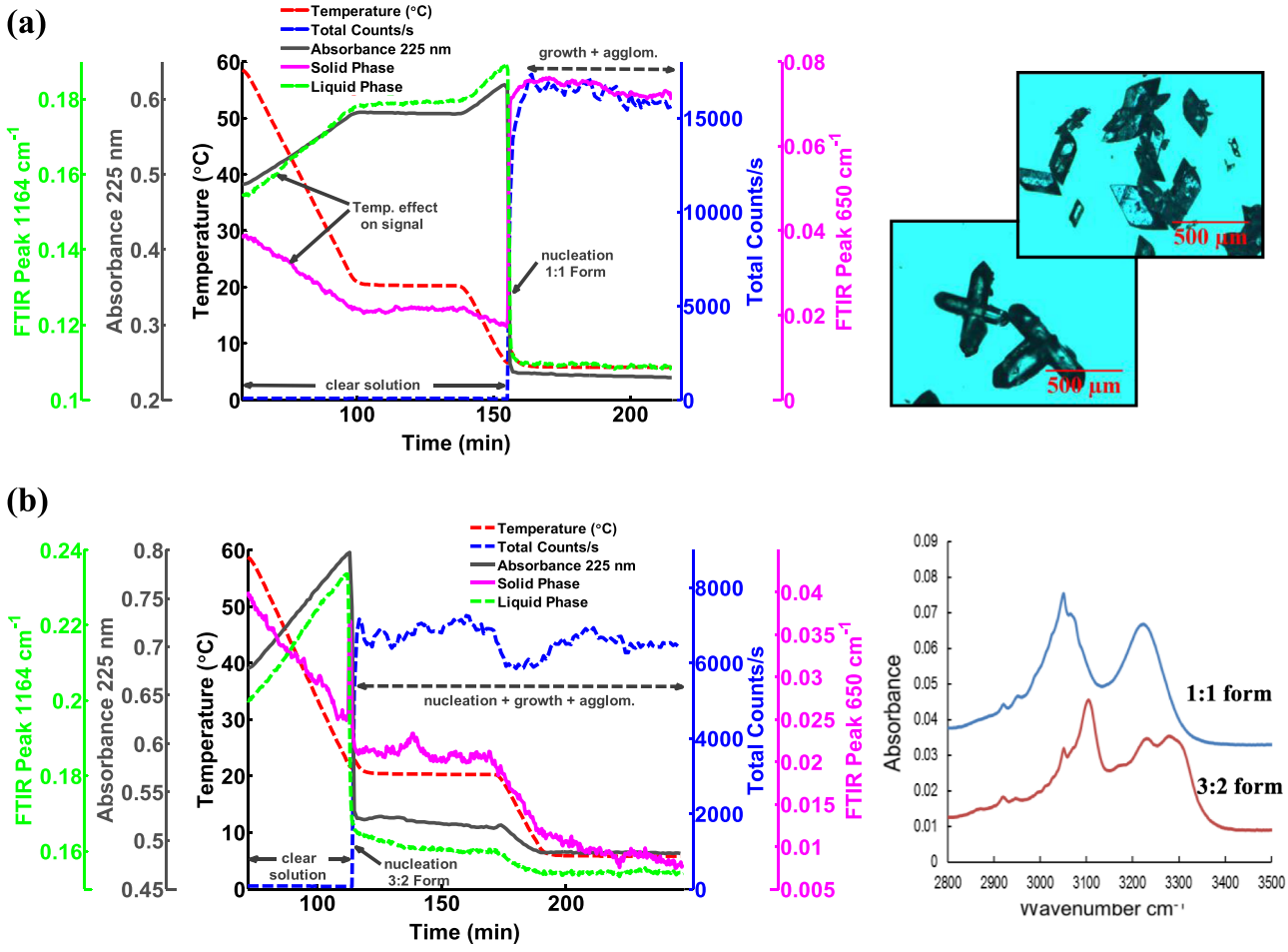

Fig. 10. Schematic showing the process time diagrams with temperature, ATR-UV/vis, ATR-FTIR and FBRM signals for the crystallization of 1:1 (a) and 3:2 (b) p-TSA–TPPO along with microscope images (top right) and off-line ATR-FTIR spectra (bottom right) of samples collected at the end of both processes.

distinct rhombic morphology, while the 3:2 form exhibits a rod-like morphology. The infrared spectra of both co-crystal forms show distinct differences in the regions associated with C–H stretching (2900–3000 cm^{-1}) and N–H stretching (3000–3400 cm^{-1}) vibration frequencies (Socrates, 2001) (Fig. 10, bottom right). Off-line Raman, XRD, DSC and HPLC also confirmed the purity of each co-crystal form.

The time diagrams (Fig. 10(a) and (b)) were annotated to indicate where important events occurred during each crystallization run. The signals from each PAT show good agreement with respect to the detection of nucleation, although the ATR-UV/vis and ATR-FTIR signals are affected by temperature. Nucleation of 1:1 p-TSA–TPPO (Fig. 10(a) – experiment 1) is not observed until cooling toward 5 °C (at approximately 6.5 °C). On the other hand, nucleation of 3:2 p-TSA–TPPO (Fig. 10(b) – experiment 2) occurs at approximately 21 °C. This was due to the difference in mass fraction composition of p-TSA/TPPO/MeCN, that is, 0.09/0.12/0.79 (experiment 1 – 1:1 p-TSA–TPPO) and 0.19/0.09/0.72 (experiment 2 – 3:2 p-TSA–TPPO). The corresponding supersaturation (S) values for the experiments 1 and 2 were 2.29 and 2.69, respectively (i.e. based on solubility of 1:1 p-TSA–TPPO at 20 °C). The cooling rate was held constant for experiment 1 and 2, respectively (see Table 1) and the overall temperature profile was the same. These experiments were found to be reproducible, in terms of the co-crystal outcome. In addition to detecting signal from the solution phase, the ATR-FTIR probe was also able to detect the solid phase signal consistently, albeit at the lower limit of the instrument (650 cm^{-1}) when 1:1 p-TSA–TPPO nucleated. This is not entirely surprising since it is well known that ATR-FTIR can be affected by particle scattering (Kadam et al., 2010; Braatz and Nagy, 2012), and to a much greater extent than ATR-UV/vis, which shows much less sensitivity (Thompson et al., 2005). However, the ATR-FTIR signal observed for the 3:2 co-crystal experiment (Fig. 10(b) – experiment 2) cannot be properly interpreted, as it was found to change in almost exactly the same way as the temperature profile, that is, except for a sudden spike in the 650 cm^{-1} peak signal at approximately 110 min. The spike was consistent with a sudden increase in FBRM counts/s and a simultaneous drop in ATR-UV/vis absorbance, with confirmation of the presence of crystals obtained via real-time PVM measurements. The change in behavior of the 650 cm^{-1} peak signal is attributed to material sticking on the probe window leading to observed change in the signal behavior. Furthermore, peaks that are close to the limits of the ATR-FTIR range (for the study the instrument had a range 650–2800 cm^{-1}) are often not consistent due to small signal to noise ratio, and therefore their reliability for interpretation of process behavior is strongly cautioned.

The mass fraction of MeCN was fixed to 0.50 for experiments 3 and 4 (Table 1) and the amount of p-TSA and TPPO varied according to the recipe by Croker et al. (2012) for obtaining pure 3:2 and 1:1 p-TSA–TPPO respectively by cooling crystallizations at 50 mL scale. For the respective experimental runs (3 and 4), pure 3:2 and 1:1 p-TSA–TPPO were obtained, as confirmed by off-line analysis (HPLC, Raman microscopy, off-line ATR-FTIR, SEM and DSC). However, due to the high solubility of p-TSA and TPPO in MeCN, it seems impractical to consider scale-up of the co-crystallization process applying the conditions used for experimental runs 3 and 4, since the high viscosity of the slurry at these high concentrations leads to poor mixing and suspension of the crystals. Furthermore, speciality agro chemicals are often highly toxic and expensive, plus the bulk storage of materials could pose health and environmental risks (Lamberth et al., 2013). Therefore, the co-crystallization was investigated at much lower concentrations of p-TSA and TPPO in MeCN (see Table 1), exploiting the upper most regions (toward MeCN) of the ternary phase diagram. Table 3 provides a summary of the outcomes in terms of co-crystal form obtained, based on-line (in situ Raman) and off-line (Raman microscopy, off-line ATR-FTIR, SEM and DSC) analyses.

The expected results in terms of co-crystal form were obtained for each composition of p-TSA/TPPO/MeCN investigated, with the exception of experiments (7) and (8). For these identical experimental runs, 3:2 and 1:1 p-TSA–TPPO respectively were initially obtained. The likely reason for this is the operation of the process in a region where both 1:1 and 3:2 p-TSA–TPPO were most likely to nucleate (i.e., region 3 of Fig. 2 as a guide) and co-exist as a mixture. These two identical experiments (note that temperature cycling was applied to (7) later) were expected to yield a mixture of 1:1 and 3:2 p-TSA–TPPO. Instead, 3:2 p-TSA–TPPO and 1:1 p-TSA–TPPO were obtained from experiments (7) and (8), respectively. The initial outcomes perhaps highlights variability issues that can arise in a batch process. It must be noted that the experimental conditions employed for runs (7) and 8 reflect the dynamics of the crystallization kinetics of the co-crystal system. The ternary phase diagram on the other hand reflects the thermodynamic stability at a fixed temperature of 20 °C. If the crystallizer was held for a long period (e.g. 24 h) at 20 °C, then perhaps a mixture of the two co-crystals would have prevailed in experiments (7) and (8). Temperature cycling was later applied to the initial product from experiment (7) and this led to a transformation from 3:2 to 1:1 p-TSA–TPPO. As demonstrated here, temperature cycling can be applied as an effect control strategies to direct the co-crystallization toward a decided outcome and within a short time period. Temperature cycling approach using active polymorphic feedback control based on in situ Raman spectroscopy is a promising method recently explored by Simone et al. (2014) to eleminate the undesired polymorph (form II) of orthoaminobenzoic acid (OABA) and then grow the desired form I. In this study, a simple temperature cycling approach was employed to eleminate the undesired 3:2 stoichiometric form of p-TSA–TPPO and grow the desired 1:1 form from experiments (6) and (7). The

Table 3
Summary of co-crystallization outcomes for the experiments 1–10, co-crystal form determined by on-line and off-line measurements.

Exp no.	p-TSA (g/g MeCN)	TPPO (g/g MeCN)	Component mass fractions (M)			HPLC ratio p-TSA/TPPO	p-TSA–TPPO co-crystal form	Region of phase diagram at 20 °C
			p-TSA	TPPO	MeCN			
1	0.1147	0.1532	0.09	0.12	0.79	1.034	1:1	2 (1:1 form)
2	0.2634	0.1247	0.19	0.09	0.72	1.486	3:2	1 (3:2 form)
3	0.5776	0.4202	0.29	0.21	0.50	1.470	3:2	1 (3:2 form)
4	0.3793	0.6193	0.19	0.31	0.50	1.002	1:1	2 (1:1 form)
5	0.0706	0.1059	0.06	0.09	0.85	1.000	1:1	2 (1:1 form)
(6)	0.1728	0.0617	0.14	0.05	0.81	1.477⇒1.002	3:2⇒1:1	1 (3:2 form)
(7)	0.1049	0.0968	0.09	0.08	0.83	1.463⇒0.998	3:2⇒1:1	3 (mixture)
8	0.1084	0.0964	0.09	0.08	0.83	1.006	1:1	3 (mixture)
9	0.0833	0.1071	0.07	0.09	0.84	1.002	1:1	2 (1:1 form)

( ) Temperature cycles implemented to convert from 3:2 to 1:1 p-TSA–TPPO. ⇒Direction of transformation on implementation of temperature cycles.

1:1 co-crystal form is desired since the 3:2 form exhibits incongruent dissolution behavior in MeCN (Croker et al., 2012, 2013b). These experiments also shed light on the stability and by extension the thermodynamics of the crystallization of 1:1 and 3:2 p-TSA–TPPO, respectively. The temperature cycles in experiments (6) and (7) were implemented based on the in situ Raman signal of peaks associated with the 3:2 and 1:1 p-TSA–TPPO co-crystal forms, respectively.

Fig. 11 shows the process time diagram for the crystallization of 3:2 p-TSA–TPPO during experiment (7). The mixture was heated up and subjected to a complex temperature profile with ramped heating and cooling cycles (Fig. 11). The same temperature profile was used for experiment (6). The final product obtained from the experiments (6) and (7) was pure 1:1 p-TSA–TPPO, as confirmed by on-line Raman spectroscopy and the off-line solid state characterization methods described earlier.

Fig. 11 also shows the point where the first sample was taken from the process (arrow 1; image S1). The sample taken was confirmed to be pure 3:2 p-TSA–TPPO by both on-line and off-line measurements. Following on from that point is the dissolution of 3:2 p-TSA–TPPO (arrow 2, image S2), which is marked by a decrease in the FBRM counts/s and the 2nd derivative of Raman peak signal at 304 cm^{-1}. Subsequent to this event, nucleation of 1:1 p-TSA–TPPO occurs (arrow 3), marked by an sudden increase in FBRM counts/s and the 2nd derivative of Raman peak signal 1145 cm^{-1}. This is followed by slight dissolution as the temperature heating cycle continues (arrow 4). At approximately 270 min there is a rapid increase in the FBRM counts/s and simultaneous increase in the 2nd derivative 1145 cm^{-1} peak signal (arrow 5; image S3) due to implementation of a temperature cooling cycle. This is attributed to secondary nucleation of 1:1 p-TSA–TPPO as the amount of 3:2 p-TSA–TPPO diminishes.

The relative solubility of each co-crystal phases plays an important role in the conversion between forms. The 3:2 co-crystal is known to undergo incongruent dissolution, whereby there is a transformation step involving the formation and subsequent dissolution of 1:1 p-TSA–TPPO (Maher et al., 2012). The temperature cooling step implemented from approximately 334 to 490 min (cooling rate of −0.2 °C/min) led to further secondary nucleation of 1-1 p-TSA–TPPO (arrow 7). The microscope image of sample 3, Fig. 11 (image S3), shows there is a mixture of 3:2 and 1:1 p-TSA–TPPO. The presence of a mixture was also confirmed by off-line solid state characterizations and HPLC analysis. Following this, a temperature heating step was implemented (heating rate of 0.2 °C/min) to dissolve 3:2 p-TSA–TPPO (arrow 8; image S3). This was then followed by another cooling step to nucleate and grow 1:1 p-TSA–TPPO (arrow 10; image S4). The final sample collected at the end of the batch (image S5) was found to be pure 1:1 p-TSA–TPPO.

The work presented here is a proof of concept study whereby the mass faction composition and temperature cycling are applied to control the co-crystallization process in order to obtained the desired stoichiometric form of the p-TSA–TPPO co-crystal system. It has been demonstrated that the co-crystal form can be controlled by manipulating the composition of p-TSA, TPPO and MeCN, as previously demonstrated by Croker et al. (2012, 2013b) in small scale studies. The stoichiometric purity of the final co-

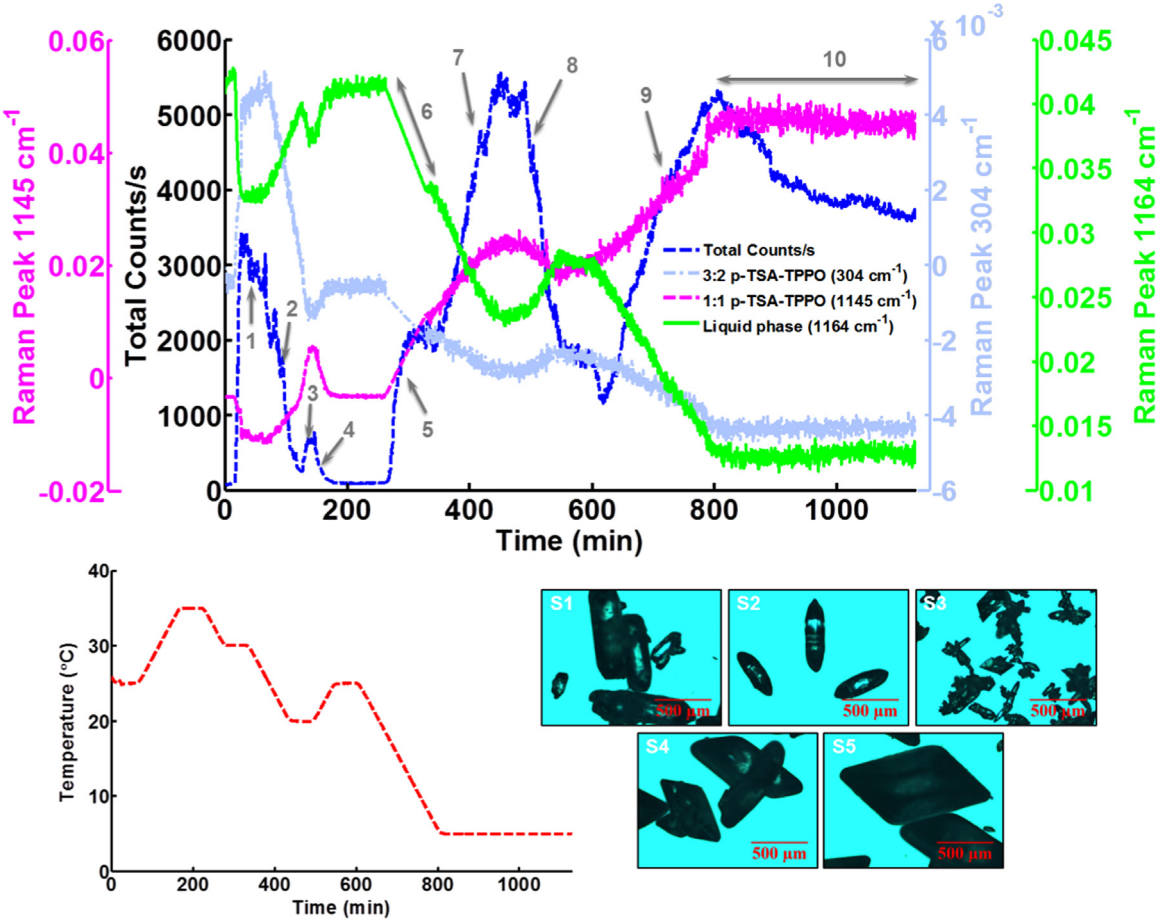

Fig. 11. Process time diagram for experiment (7) showing the changes in FBRM count/s and in situ Raman 2nd derivative signals (top), temperature profile implemented (bottom left) and microscope images of samples (bottom right). 1=Sample 1 at 57 min, 2=Sample 2 at 109 min, 3=Nucleation event, 4=Dissolution event, 5=Sample 3 at 272 min, 6=Signal loss/fluorescence, 7=Nucleation event, 8=Sample 4 at 177 min, 9=Nucleation event, 10=Sample 5 at 1137 min. **Growth/agglomeration/settling observed.

crystal was assured by implementation of a complex array of on-line and off-line monitoring and characterization techniques. Also demonstrated is the application of a complex temperature profile having several heating and cooling cycles to influence the outcome of the co-crystallization when the undesired form is initially obtained. The process was also characterized using a combination of on-line and off-line PAT tools. Attempts to convert from 1:1 to 3:2 p-TSA–TPPO were unsuccessful, however, studies are ongoing to investigate if this is possible using the same scale of equipment used in this study.

3.4. Semi-batch co-crystallization monitoring and control

The semi-batch co-crystallization of p-TSA with TPPO was explored under flow conditions whereby a fixed concentration of the two starting materials dissolved in MeCN are pumped separately, then combined and mixed in a batch crystallizer (see Fig. 4). In this study the flow rates of the two components were adjusted to crystallize the desired stoichiometric form of the p-TSA–TPPO co-crystal system. This operating strategy offers a promising alternative to batch, and could potential lend itself to further development into a continuous co-crystallization operation. Table 4 provides a summary of the co-crystallization outcomes for each of the semi-batch experimental runs.

Fig. 12 (a) and (b) shows the process time diagrams with temperature profile and on-line PAT signals from FBRM (solid phase), ATR-UV/vis (solution phase), ATR-FTIR (solution phase) and Raman (co-crystal form and solution phase monitoring) for experiment 10. The co-crystal form obtained from this experiment was pure 3:2 p-TSA–TPPO as confirmed by both on-line (Raman MR immersion probe) and off-line (HPLC, PXRD, Raman microscope and ATR-FTIR) measurements. Experiments 11–17 (Table 4) were carried out under similar process conditions to experiment 10, meaning the process temperature (varying from 25 °C to 20 °C) and concentrations of p-TSA (0.2987 g/g MeCN) and TPPO (0.1492 g/g MeCN) in the feed vessels were exactly the same. The main difference between these runs is the mass flow rate of p-TSA and TPPO from the feed vessels (Fig. 4) to the crystallizer. The results show that by changing the mass flow rate of either p-TSA or TPPO, one can change the mass fraction composition of materials in the crystallizer and thereby control the co-crystallization outcome. When the flow rate is adjusted so that the mass fractions of p-TSA and TPPO are similar, the resulting mixture falls into region 3 of the ternary phase diagram and hence two co-crystal forms were obtained, for example, as observed from experiments 12 and 16 (Table 4).

Indeed, the semi-batch co-crystallization experiments were more consistent in terms of co-crystallization outcomes when compared to the batch runs described earlier (Section 3.2). Moreover, slight changes in the mass flow rate of one or both co-formers can alter the co-crystallization outcome favoring either 1:1 or 3:2 p-TSA–TPPO or a mixture. However, these changes can be avoided if the flow rates are controlled appropriately.

3.5. Principal component analysis on in situ Raman spectra

Principal component analysis (PCA) is often used in chemometrics to extract the dominant patterns from chemical data. The result is a complementary set of scores and loadings that can be used to visualize trends in the data (Wold et al., 1987). PCA analysis was performed on the Raman spectra obtained when pure 1:1 and 3:2 p-TSA–TPPO and mixture of the two co-crystals forms nucleated; a total of 390 spectra obtained from the batch and semi-batch experiments described earlier. Fig. 13 shows the scores plot of principal components 1 and 2 obtained from the analysis. It shows there are three clusters of data corresponding to each of the three experimental runs. Analysis of the PCA scores plot allows for the identification of the co-crystal form obtained from each of the experimental runs. PC1 and PC2 combined represent 93.2% of the spectral variance. The three distinct clusters indicate that a different co-crystal form or a mixture of forms was obtained from each experimental run. Clusters 1, 2 and 3 represent experiments 10, 12 and 13 respectively, and the co-crystal forms were 3:2, mixture of 1:1 and 3:2, and 1:1 p-TSA–TPPO respectively. Arrows show the direction of increasing amount of solids as the crystallization progresses. PCA is an additional tool that was used to monitor and characterize the co-crystallization process, providing valuable information pertaining to the crystalline form that nucleates and grows.

4. Conclusions

In this study, the cooling co-crystallization of p-TSA with TPPO to form either the 1:1 or 3:2 p-TSA–TPPO stoichiometric co-crystal from MeCN was demonstrated in laboratory scale 500 mL batch and semi-batch crystallizers. Monitoring and control of the selective co-crystallization of 1:1 and 3:2 p-TSA–TPPO was achieved using an integrated array of PAT tools complemented by off-line solid state characterization techniques. These technologies allowed gave a better understanding of the co-crystallization process. Three different regions of the p-TSA/TPPO/MeCN ternary phase diagram corresponding to the formation of the pure co-crystals as well as mixtures of both forms were explored by changing the mass fraction compositions of p-TSA/TPPO/MeCN in the crystallizers.

In the batch study, as expected the pure 1:1 and 3:2 co-crystal forms were successfully isolated when the process was operated well within the respective stable regions extrapolated from the ternary diagram at 20 °C. However, batch-to-batch variability issues were occasionally encountered when the process was operated in the mixture region. It was demonstrated that if temperature cycling

Table 4
Summary of co-crystallization outcomes for the experiments 10–17, co-crystal form determined by on-line and off-line measurements.

Exp no.	Solution flow rates (g/min)		Mass fractions (M) in crystallizer			HPLC ratio p-TSA/TPPO	p-TSA–TPPO co-crystal form	Region of phase diagram at 20 °C
	p-TSA soln.	TPPO soln.	p-TSA	TPPO	MeCN			
10	28.0	24.7	0.12	0.09	0.79	1.479	3:2	1 (3:2 form)
11	32.7	20.0	0.14	0.05	0.81	1.522	3:2	1 (3:2 form)
12	20.0	32.7	0.09	0.08	0.83	1.313	1:1+3:2	3 (mixture)
13	15.0	37.7	0.06	0.09	0.85	1.002	1:1	2 (1:1 form)
14	20.0	32.7	0.12	0.12	0.76	1.021	1:1	2 (1:1 form)
15	23.4	29.3	0.10	0.08	0.83	1.475	3:2	3 (mixture)
16	17.7	35	0.08	0.08	0.84	1.333	1:1+3:2	3 (mixture)
17	27.5	25.2	0.11	0.07	0.82	1.475	3:2	1 (3:2 form)

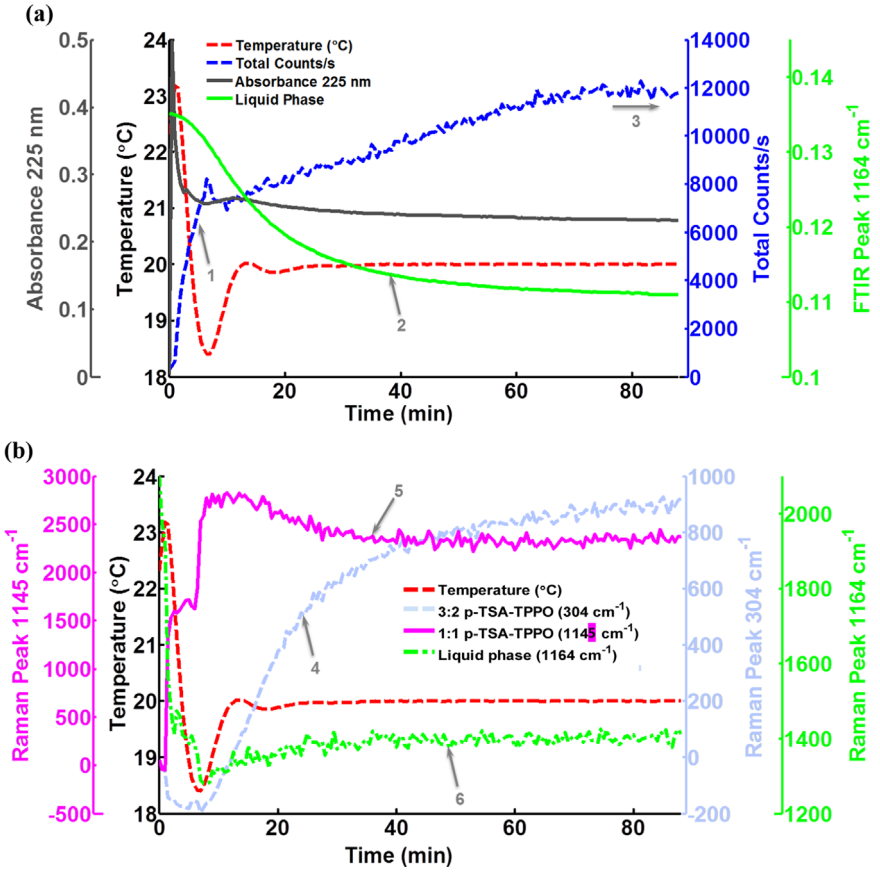

Fig. 12. Process time diagrams of experiment 10 showing the temperature profile, (a) FBRM total particle counts/s (solid phase monitoring) and the change in absorbance and peak intensity readings from ATR-UV/vis and ATR-FTIR probes used to monitor the liquid phase; and (b) changes in the 2nd derivative of Raman peaks at 1145 and 304 cm^{-1}, associated with 1:1 and 3:2 p-TSA–TPPO, respectively, and the liquid phase. Arrows show respectively, nucleation (FBRM counts/s) (1), decreasing solute in solution phase (2), crystal growth (3), increasing 3:2 p-TSA–TPPO peak (4), 1:1 p-TSA–TPPO peak (5), and change in solution phase (6).

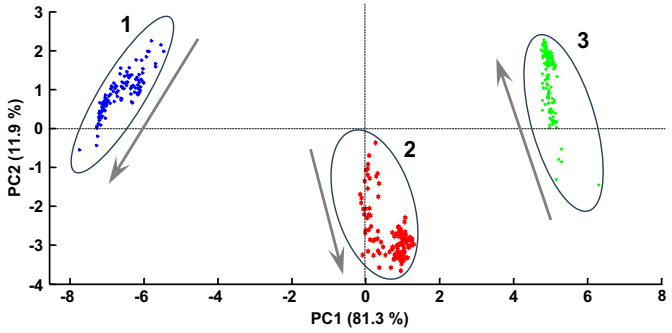

Fig. 13. PCA scores plot of Raman spectra from experimental runs 10 (cluster 1), 12 (cluster 2) and 13 (cluster 3). Arrows show the direction of increasing amounts of solids as the crystallizations progress.

is implemented with the aid of in situ Raman spectroscopy measurements and off-line solid-state characterization methods, then the crystallization can be controlled and directed towards the desired outcome, that is, to obtain the more stable 1:1 p-TSA–TPPO co-crystal. The transformation from 3:2 to 1:1 p-TSA–TPPO via temperature cycling was presented as a proof of concept approach to the control of crystalline form during co-crystallization, which prior to now was only been demonstrated for single component molecular systems. The study shows, for the first time the use of PAT to monitor the transformation events in a co-crystal system. The information was then used to aid the control of the co-crystallization process in order to obtain the desired crystalline form.

The semi-batch co-crystallization study was carried out using a fixed concentration of the two co-formers (p-TSA and TPPO) in MeCN, each prepared in a separate vessel. In this proof of concept study, the co-crystallization was controlled by changing the flow rate of the dissolved materials to the crystallizer. It was demonstrated that by changing the flow rates, the mass fraction of components sent to the crystallizer could be controlled, thereby controlling the outcome of the co-crystallization. This operation is promising, and could potentially be developed into a continuous co-crystallization process.

Acknowledgments

The authors would like to thank the EPSRC (EP/I033459/1) and the Centre for Continuous Innovation in Continuous Manufacturing and Crystallization (CMAC) for the financial support of this work and the European Research Council under the European Union's Seventh Framework Programme (FP7/2007-2013)/ERC Grant agreement no. [280106-CrySys] (for equipment and financial support). Authors would also like to acknowledge financial support from the National Science Foundation (NSF), USA and Science Foundation Ireland (SFI) through the project "US-Ireland R&D Partnership in continuous manufacturing for nano-based drug products" between the Synthesis and Solid State Pharmaceutical Cluster (SSPC), Ireland and the Centre for Structured Organic Particulate Systems (CSOPS), USA.

References

Aitipamula, S., Banerjee, R., Bansal, A.K., Biradha, K., Cheney, M.L., Choudhury, A.R., Desiraju, G.R., Dikundwar, A.G., Dubey, R., Duggirala, N., Ghogale, P.P., Ghosh, S., Goswami, P.K., Goud, N.R., Jetti, R.R.K.R., Karpinski, P., Kaushik, P., Kumar, D., Kumar, V., Moulton, B., Mukherjee, A., Mukherjee, G., Myerson, A.S., Puri, V., Ramanan, A., Rajamannar, T., Reddy, C.M., Rodríguez-Hornedo, N., Rogers, R.D., Row, T.N.G., Sanphui, P., Shan, N., Shete, G., Singh, A., Sun, C.C., Swift, J.A., Thaimattam, R., Thakur, T.S., Kumar Thaper, R., Thomas, S.P., Tothadi, S., Vangala, V.R., Variankaval, N., Vishweshwar, P., Weyna, D.R., Zaworotko, M.J., 2012. Polymorphs, salts, and cocrystals: what's in a name? Cryst. Growth Des. 12 (5), 2147–2152.

Ajibola, A., Gago-Ferrero, P., Borova, V.L., Dasenaki, M.E., Bletsou, A.A., Thomaidis, N. S., 2015. "Benzosulfonamides in wastewater: method development, occurrence and removal efficiencies. Chemosphere 119 (Suppl.), S21–S27.

Bian, L., Zhao, H., Hao, H., Yin, Q., Wu, S., Gong, J., Dong, W., 2013. Novel glutaric acid cocrystal formation via cogrinding and solution crystallization. Chem. Eng. Technol. 36 (8), 1292–1299.

Braatz, R.D., Nagy, Z.K., 2012. Advances and new directions in crystallization control. Annu. Rev. Chem. Biomol. Eng. 3, 55–75.

Croker, D.M., Davey, R.J., Rasmuson, Å.C., Seaton, C.C., 2013a. Nucleation in the p-toluenesulfonamide/triphenylphosphine oxide co-crystal system. Cryst. Growth Des. 13 (8), 3754–3762.

Croker, D.M., Davey, R.J., Rasmuson, Å.C., Seaton, C.C., 2013b. Solution mediated phase transformations between co-crystals. CrystEngComm 15 (11), 2044.

Croker, D.M., Foreman, M.E., Hogan, B.N., Maguire, N.M., Elcoate, C.J., Hodnett, B.K., Maguire, A.R., Rasmuson, Å.C., Lawrence, S.E., 2012. Understanding the p-toluenesulfonamide/triphenylphosphine oxide crystal chemistry: a new 1:1 co-crystal and ternary phase diagram. Cryst. Growth Des. 12 (2), 869–875.

Croker, D.M., Rasmuson, Å.C., 2014. Isothermal suspension conversion as a route to cocrystal production: one-pot scalable synthesis. Org. Process Res. Dev. 18 (8), 941–946.

Drebushchak, T.N., Pankrushina, N.A., Mikheev, A.N., Thumm, M.K.A., 2013. Crystalline products of tolbutamide decomposition in water after microwave treatment. CrystEngComm 15 (18), 3582.

Etter, M.C., Baures, P.W., 1988. Triphenylphosphine oxide as a crystallization aid. J. Am. Chem. Soc. 110 (2), 639–640.

Farahi, M., Karami, B., Tanuraghaj, H.M., 2015. Efficient synthesis of a new class of sulfonamide-substituted coumarins. Tetrahedron Lett. 56 (14), 1833–1836.

FDA, 2013. Guidance for Industry Regulatory Classification of Pharmaceutical Co-Crystals Guidance for Industry Regulatory Classification of Pharmaceutical Co-Crystals.

Ferguson, G., Glidewell, C., 1988. The reactions of triphenylphosphine and triphenylarsine with chloramine-T, sodium N-chlorotoluene-p-sulphonamide: crystal and molecular structure of triphenylphosphine oxide–toluene-p-sulphonamide (2/3). J. Chem. Soc. Perkin Trans. 2 (12), 2129–2132.

Ferguson, G., Lough, A.J., Glidewell, C., 1989. The reactions of triarylphosphines and triarylarsines with chloramines B and T: crystal and molecular structures of triphenylarsine oxide-benzenesulphonamide (1: 1) hemi-acetone solvate and tri-m-tolylphosphine oxide-toluene-p-sulphonamide (1: 1). J. Chem. Soc. Perkin Trans. 2 (12), 2065.

Gagniere, E., Mangin, D., Puel, F., 2009. Cocrystal formation in solution: in situ solute concentration monitoring of the two components and kinetic pathways. Cryst. Growth Des. 9 (8), 3376–3383.

Habgood, M., Deij, M.A., Mazurek, J., Price, S.L., ter Horst, J.H., 2010. Carbamazepine co-crystallization with pyridine carboxamides: rationalization by complementary phase diagrams and crystal energy landscapes. Cryst. Growth Des. 10 (2), 903–912.

Kadam, S.S., van der Windt, E., Daudey, P.J., Kramer, H.J.M., 2010. A comparative study of ATR-FTIR and FT-NIR spectroscopy for in-situ concentration monitoring during batch cooling crystallization processes. Cryst. Growth Des. 10 (6), 2629–2640.

Karki, S., Friščić, T., Jones, W., Motherwell, S.W.D., 2007. Screening for pharmaceutical cocrystal hydrates via neat and liquid-assisted grinding. Mol. Pharm. 4 (3), 347–354.

Kuntz, I.D., 1992. Structure-based strategies for drug design and discovery. Science 257 (5073), 1078–1082.

Lamberth, C., Jeanmart, S., Luksch, T., Plant, A., 2013. Current challenges and trends in the discovery of agrochemicals. Science 341 (6147), 742–746.

Maher, A., Croker, D.M., Rasmuson, Å.C., Hodnett, B.K., 2012. Solution mediated polymorphic transformation: Form II to Form III piracetam in ethanol. Cryst. Growth Des. 12 (12), 6151–6157.

Padrela, L., Rodrigues, M.A., Velaga, S.P., Fernandes, A.C., Matos, H.A., de Azevedo, E. G., 2010. Screening for pharmaceutical cocrystals using the supercritical fluid enhanced atomization process. J. Supercrit. Fluids 53 (1–3), 156–164.

Palmer, R.K., Atwal, K., Bakaj, I., Carlucci-Derbyshire, S., Buber, M.T., Cerne, R., Cortés, R.Y., Devantier, H.R., Jorgensen, V., Pawlyk, A., Lee, S.P., Sprous, D.G., Zhang, Z., Bryant, R., 2010. Triphenylphosphine oxide is a potent and selective inhibitor of the transient receptor potential melastatin-5 ion channel. Assay Drug Dev. Technol. 8 (6), 703–713.

Prasad, R., Rakesh, M., 2012. Pharmaceutical cocrystallization: a review. Int. J. Pharm. Chem. 1 (3), 725–736.

Rager, T., Hilfiker, R., 2010. Cocrystal formation from solvent mixtures. Cryst. Growth Des. 10 (7), 3237–3241.

Richoll, S.M., Colón, I., 2006. Determination of triphenylphosphine oxide in active pharmaceutical ingredients by hollow-fiber liquid-phase microextraction followed by reversed-phase liquid chromatography. J. Chromatogr. A 1127 (1–2), 147–153.

Sarraguça, M.C., Ribeiro, P.R., Santos, A., Silva, M.C., Lopes, J.A., 2014. A PAT approach for the on-line monitoring of pharmaceutical co-crystals formation with near infrared spectroscopy. Int. J. Pharm. 471 (1–2), 478–484.

Simone, E., Saleemi, A.N., Tonnon, N., Nagy, Z.K., Saleemi, Ali N., Tonnon, N., Nagy, Z. K., 2014. Active polymorphic feedback control of crystallization processes using a combined raman and ATR-UV/vis spectroscopy approach. Cryst. Growth Des. 14, 1839–1850.

Socrates, G., 2001. Infrared and Raman Characteristic Group Frequencies: Tables and Charts, third ed. Wiley, Chichester.

Spek, A.L., 1987. Structure of a second monoclinic polymorph of triphenylphosphine oxide. Acta Crystallogr. Sect. C: Cryst. Struct. Commun. 43 (6), 1233–1235.

Sun, C.C., 2013. Cocrystallization for successful drug delivery. Expert Opin. Drug Deliv. 10 (2), 201–213.

Takata, N., Shiraki, K., Takano, R., Hayashi, Y., Terada, K., 2008. Cocrystal screening of stanolone and mestanolone using slurry crystallization. Cryst. Growth Des. 8 (8), 3032–3037.

Thompson, D.R., Kougoulos, E., Jones, A.G., Wood-Kaczmar, M.W., 2005. Solute concentration measurement of an important organic compound using ATR-UV spectroscopy. J. Cryst. Growth 276 (1–2), 230–236.

Varghese, J.N., 1999. Development of neuraminidase inhibitors as anti-influenza virus drugs. Drug Dev. Res. 46 (3–4), 176–196.

Walmsley, S., Bernstein, B., King, M., Arribas, J., Beall, G., Ruane, P., Johnson, M., Johnson, D., 2002. Lopinavir–ritonavir versus nelfinavir for the initial treatment of HIV infection. N. Engl. J. Med. 346, 2039–2046.

Wold, S., Esbensen, K., Geladi, P., 1987. Principal component analysis. Chemom. Intell. Lab. Syst. 2 (1–3), 37–52.

Yu, Z.Q., Chow, P.S., Tan, R.B.H., Ang, W.H., 2011. Supersaturation control in cooling polymorphic co-crystallization of caffeine and glutaric acid. Cryst. Growth Des. 11 (10), 4525–4532.